Dual-chamber ultra line-narrowed excimer light source for 193 nm lithography

V.B. Fleurov, D.J. Colon III, D.J.W. Brown, P. O'Keeffe, H. Besaucele, A.I. Ershov, F.Trinchouk, T. Ishihara, P. Zambon, R. Rafac, A. Lukashev

Cymer, Inc.
16750 Via Del Campo Court, San Diego CA 92127 USA

ABSTRACT

Since the announcement in March 2002 of plans to develop an advanced light source to meet the future spectral power and cost requirements of photolithography, we have made significant progress in the development and productization of the core technology for an ultra line-narrowed, excimer light source based on a master oscillator-power amplifier (MOPA) approach. In this paper, we will focus on the architecture and performance of the first generation of production-ready, MOPA-based ArF light sources developed at Cymer, Inc. This first generation of MOPA-based ArF light sources is referred to as the XLA 100 product series.

Keywords: Excimer laser, 193nm light source, narrow bandwidth, MOPA, DUV, Microlithography

1. INTRODUCTION

The XLA 100 is Cymer's new, ultra line-narrowed, high power argon fluoride production laser system based on Master Oscillator Power Amplifier design. Generating a 193 nm exposure wavelength, the XLA 100 enables micro chip design scale to shrink, compared to 248nm (KrF) sources which leads to faster processing speeds and boosts memory capacity per chip. With an ultra line-narrowed spectral bandwidth typically below 0.2 pm FWHM, the XLA 100 matches requirements for high contrast imaging microlithography with a numerical aperture (NA) values higher than 0.9.

Splitting the functions of generating the required spectral bandwidth, and generating the stable high power output has essential advantages for lithography light source design compared to a singe chamber design. In MOPA configuration, line-narrowing optics operate at much lower fluencies than in a single-oscillator system, decreasing optically induced heating effects and prolonging lifetime [1,2]. Further, the master oscillator only needs to generate low pulse energy, enabling easier achievement of ultra-narrow bandwidth. Another advantage of utilizing a two-stage MOPA architecture is that the power amplifier can be operated in a well-saturated regime, which allows improved energy and dose control. Finally, the MOPA architecture has tremendous operational efficiency and robustness, which can translate into lifetime extension.

The XLA 100 series has a new, more powerful control system built on a new platform, which is universal for all XL series products. The "laser firing" part of the control system incorporates pulse-by-pulse output energy and wavelength control capabilities as in Cymer's previous 7000 series of excimer light sources, but contains the additional key capability of gas discharge synchronization. Pulse energy measurements at the master oscillator and power amplifier output are used for independent control of F_2 concentration in the two discharge chambers.

XLA-100 ARCHITECTURE

The optical layout of XLA -series of MOPA systems is shown in Figure 1. The dual chamber configuration utilizes similar chamber design as in the 7000A series with improved gas flow-dynamic and acoustics properties. The same chamber type in used for Master Oscillator (MO) and Power Amplifier (PA).

Optical Microlithography XVI, Anthony Yen, Editor, Proceedings of SPIE
Vol. 5040 (2003) © 2003 SPIE · 0277-786X/03/$15.00

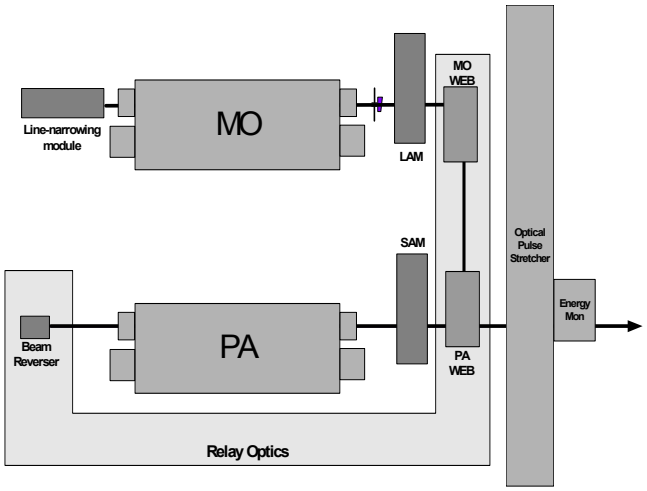

Fig. 1. Optical architecture of XLA-100

The MO, on the top, produces narrow bandwidth output (typically <0.2pm FWHM) within 0.5-1.5mJ energy range. It has a two level wavelength control, provided by the stepper motor (coarse) and PZT (fine) actuators, similar to the Nanolith 7000 models[3]. Relay optics in the MO WEB, PA WEB and beam reverser modules direct the MO light on a double pass through the PA. The dual pass amplification scheme in PA is highly desirable because it allows to utilize gain saturation effects in PA to positively affect the output energy stability.

The amplified radiation exiting the PA is propagated through the second relay optics module optics module, PA WEB where the spatial pulse width is expanded in horizontal direction using anamorphic beam expansion technique. The Optical Pulse Stretcher extends the temporal pulse width using optical delay lines. As a result, the peak optical power of the 10mJ stretched pulses is maintained at approximately the same levels as for the 5mJ output of a single-oscillator excimer system.

The Line-Center Analysis Module (LAM) monitors output wavelength and pulse energy of the MO and provides wavelength auto-calibration procedure using Pt lamp as an absolute wavelength reference source. The Spectral Analysis Module (SAM) monitors high-resolution FWHM bandwidth and PA output energy. The system output energy is monitored downstream from the pulse stretcher inside the beam auto-shutter module. The auto-shutter module contains an internal power head that can be inserted into the beam path to execute an auto-calibration procedure of the output power photo detector.

The pulsed power architecture of XLA100 series utilizes a single, resonantly charging power supply and a single commutator that supplies operational pulsed voltage to MO and PA chambers through two independent commutators. Both chambers are operated at the same well controlled voltage.

A new feature of the XLA 100 control system is precise discharge synchronization, that allows to keep constant delay between triggering discharges in MO and PA chambers, regardless of applied voltage. The operating point of the delay control corresponds to maximum efficiency of the system, as shown in Fig. 2. The accuracy of synchronization control in XLA 100 system is better than 2ns, to ensure that timing stability does not impact accuracy of the energy control.

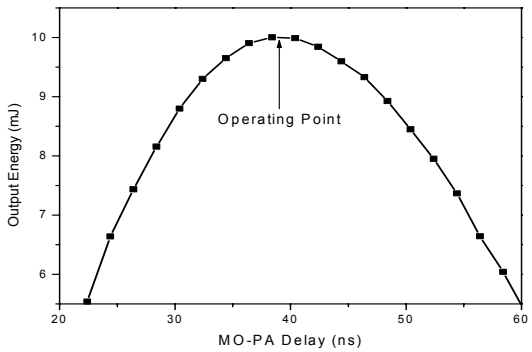

Fig.2. Output energy vs relative MO-PA timing

TOP LEVEL OPTICAL PERFORMANCE

XLA 100 light sources operate in a 500-4000 Hz repetition rate at average output power of 40W. The maximum duty cycle at 4000Hz is 75%. The energy dose stability, measured for a 20ms moving average window, is better than 0.3%. Fast pulse-to-pulse wavelength control, based on a PZT actuator, provides instantaneous wavelength adjustment within and between the bursts (open loop control), and high stability of line center position within a 20 fm accuracy.

The fraction of amplified spontaneous emission in the XLA-100 output is insignificant and does not exceed $0.5x10^{-4}$ of the energy output. Our recent studies showed [2] that fractional energy content of ASE pedestal in output spectrum of the MOPA system strongly depends on discharge delay and reaches its minimum at the optimal efficiency and can be maintained below 10^{-4} level within ± 10 ns error margin of the discharge synchronization.

Optimization of LNM design dramatically reduced spectrum width down to 0.2pm FWHM and 0.5pm E95% typical values.

Top level optical performance, applied for 1500-4000 operational range and output pulse energy range between 8.5-11.5mJ is summarized in Table 1

Table 1

Parameter	Value
Average Output Power	40W
Maximum repetition rate	4kHz
Energy Dose stability (20ms window)	<0.3%
Nominal Pulse Energy	10mJ
Maximum Operational Pulse Energy	11.5mJ
Minimum Operational Pulse Energy	8.5mJ
Peak energy density	$30mJ/cm^2$
Temporal pulse width (Integral Square definition)	>45ns
Nominal Wavelength	193.368nm
Wavelength Tuning Range	193.200nm-193.500nm
Spectral width FWHM	<0.25pm
Spectral Width E95%	<0.65pm
Short term Wavelength stability (20ms window)	Better than ± 20fm
Gas life	100M shots, 36 hours

BEAM CHARACTERISTICS AND OUTPUT POWER

One of the most sensitive requirements to the development of powerful 193-nm sources for lithographic application is a reduction of the intensity and peak energy density of the output beam[4]. Temporal pulse width of XLA-100, equipped with the optical pulse stretcher is increased more than two times compared to the Nanolith 7000 systems. The output pulse from an XLA-100 laser is overlaid Nanolith 7000 laser in Fig.3 for comparison, indicating that the peak optical power in both cases is similar.

In addition, peak energy density in XLA-100 system is decreased to $30mJ/cm^2$ compared to Nanolith 7000 ($<50mJ/cm^2$), as a result of beam expansion in horizontal plane, in PA WEB module. As shown in fig 4, the output beam has a square footprint, determined by the output aperture of $12x12mm^2$. The peak energy density may slightly vary with the repetition rate, but remains typically around 20 mJ/cm^2.

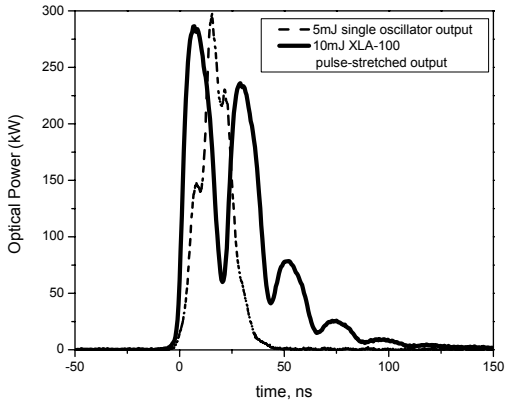

Fig.3. Temporal pulse shape of output
comparison between XLA100 model (10mJ, 4kHz)
and a single-chamber Nanolith 7000 model (5mJ, 4kHz)
the multi-hump structure of 10mJ pulse is
due to multiple beam passes inside the
pulse stretcher

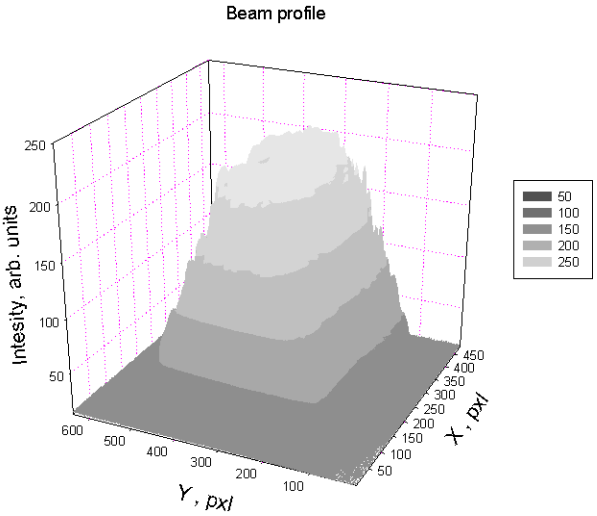

Fig.4. Output beam profile captured shape,
with CCD camera at 400Hz
Beam footprint has a square shape, 12x12mm^2
Peak E density =17mJ/cm^2

One of the advantages of MOPA system is tremendous output power overhead. The efficiency curves (power versus operating voltage) shown in the Fig. 5 indicate that MOPA output can be varied within a wide dynamic range, exceeding 60 mJ pulse energy. However, a required level of intrinsic energy stability of MOPA system at fixed gas fill conditions can be maintained only within a narrower dynamic range of output energy. The actual operational range corresponds to the right hand side E(V) curve, which allows to utilize saturation effect of PA gain and better intrinsic energy stability of MO. High level of energy stability can be maintained approximately within ±20% from the optimum output energy level. For higher nominal output energy the higher total fill pressures of PA are required.

The output energy and energy stability of XLA100 system at various PA pressure fills is shown in Fig.6. These results illustrate that maximum standard deviation of output energy remains at the same level of ~1-1.2%, when the nominal output energy is varied from 16 to 30mJ. One of the most important applications of the gas fill re-optimization procedure is to boost the efficiency of aging chambers and as a result, to increase the life time of XLA-100 systems. We are planning to perform this study in near future.

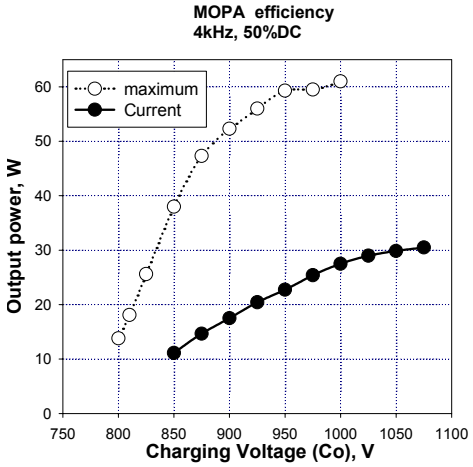

Fig.5 Energy versus Voltage curves for XLA-100 . For the curve marked 'Current', the MO chamber operates at optimal efficiency, the PA efficiency is changed using different PA gas fills

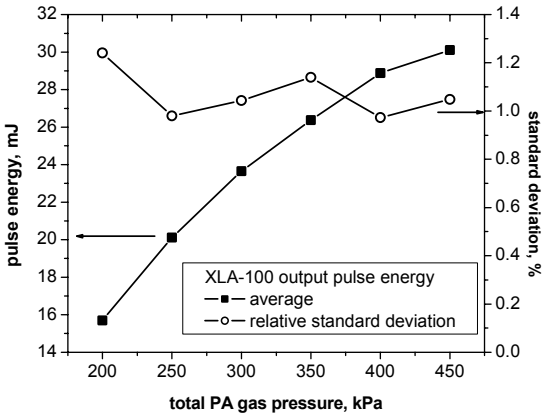

Fig.6. Pulse energy and Energy stability
(measured as a standard energy deviation, %)
vs total pressure fill in PA.
F_2 concentration was also adjusted at each data point
E stability measured as max value for each pulse.

SPECTRAL WIDTH OF XLA-100 OUTPUT AT VARIOUS REPETITION RATES

Our earlier studies [5] illustrated that MOPA bandwidth at optimal MO-PA delays, shown in Fig.2, is determined by MO performance. Spectroscopic measurements on XLA-100 system were performed with fully reflective grating spectrometer ELIAS-II, (Laser Technik, Berlin). The slit function of the spectrometer was measured at 193nm using injection-seeded solid-state laser system. Evaluation of the bandwidth performance of the XLA-100 system over the operational repetition rate range was performed in burst mode, with 1200 pulses per burst and a 0.1 second inter-burst intervals. The repetition rate was changed by 10 Hz increments in 2000-4000Hz range. Three successive measurements were taken at each repetition rate. A specially developed Fourier-transform-based procedure for deconvolution of FWHM and of the spectral integral (E95%) was applied. The raw spectroscopic data were post-processed using a LabView code, which allowed to deconvolve all 750 spectra within ~ 40 min.

The raw (convolved) measurements of FWHM and E95% values and results of their deconvolution are shown in figures 7 and 8. Both values stay well within ranges specified in Table 1. Comparing convolved and deconvolved FWHM values one can find that deconvolution procedure takes off ~0.02pm in the valleys and only ~0.01 pm at the

peaks. Overall variation of XLA 100 spectral width in 2000-4000 Hz repetition range is within 0.11-0.20 pm for FWHM and 0.28-0.38 pm for E95%. One can note that both FWHM and E95% values show increasing variation at higher repetition rates.

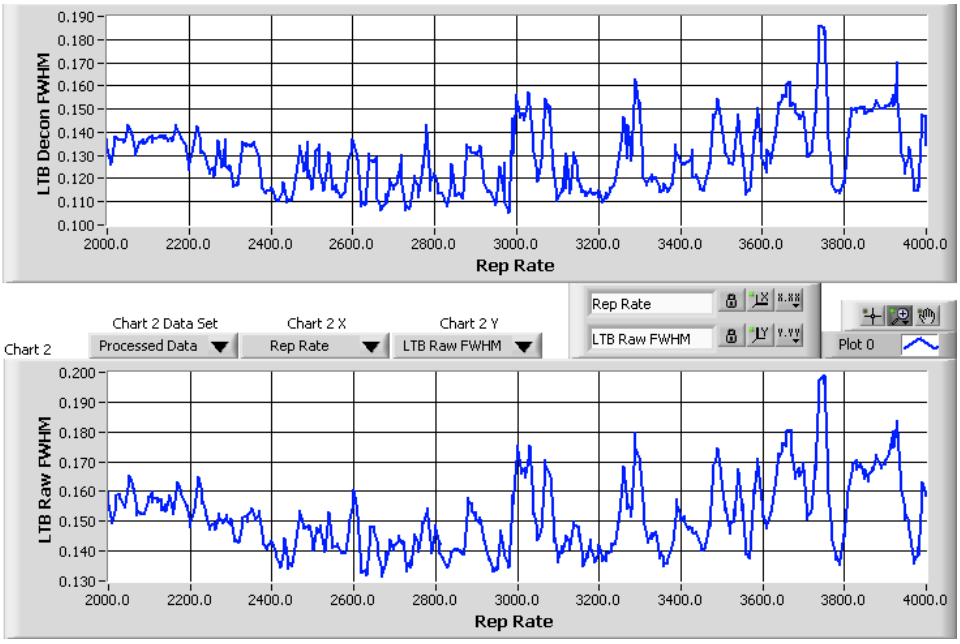

Fig.7. Deconvolved and convolved FWHM measurements of XLA-100 output in 2000-4000Hz range

The nature of these variations is well understood now and is explained by acoustic effects in MO chamber[6]. The acoustic origin of the bandwidth spikes can be verified by changing the gas temperature in MO chamber. As a result the position of the bandwidth spikes Δf(Hz)=f1-f2 shifts proportionally to the change of gas velocity in MO, following the relationship:

$$f2/f1=\{(T1+273^0C)/(T2+273^0C)\}^{1/2},$$

where f1 and f2 are to the positions of selected spikes in frequency domain, T1 and T2 are the corresponding MO gas temperatures in C^0. We did not see the acoustic effects to the output bandwidth from PA chamber.

In accordance with our studies, the acoustic effects below 2kHz are weak and show no significant bandwidth spikes. Contrary, at repetition rates above 4kHz, direct reflections from the electrodes surfaces and from the near electrodes features of the chamber interior can significantly distort the bandwidth performance. Strong bandwidth spikes at high rep rate distortion cannot be easily mitigated by application of acoustic absorbers in the chamber. This can be a serious challenge for the development of ultra-narrow bandwidth 6kHz laser systems.

ENERGY STABILITY AND WAVELENGTH STABILITY

The results of a 75M shot long operation of XLA 100 various firing modes and duty cycles at 4kHz are shown in the figures 9 and 10. Various burst modes and duty cycles from 6% to 75% were tested.

Fig. 9 shows the evolution of the operational voltage with shots count and illustrates the effect of duty cycle change to the operating voltage. The overall voltage variation over 75M shots is about 74V, and is effected by the duty cycle change, as well as by the aging of the gas mixture. At high duty cycles the efficiency of the chambers increases that cause a slight voltage drop at low-to-high DC change and vise versa. After gas refill the starting voltage recovers to initial values. The operational range of the XLA-100 system is 850-1150V.

The automatically controlled F_2 injections were performed simultaneously in both chambers. The size of injects to MO and PA chambers was determined by the laser control system using estimation of active and passive F_2 consumption in each chamber.

The energy dose stability performance is shown in the upper graph, Fig.10 (upper graph). Maximum and minimum dose errors for 80p moving average window (20ms) are below 0.1%. The auto inject occurrences, shown on the same graph, do not disturb the energy stability of the laser.

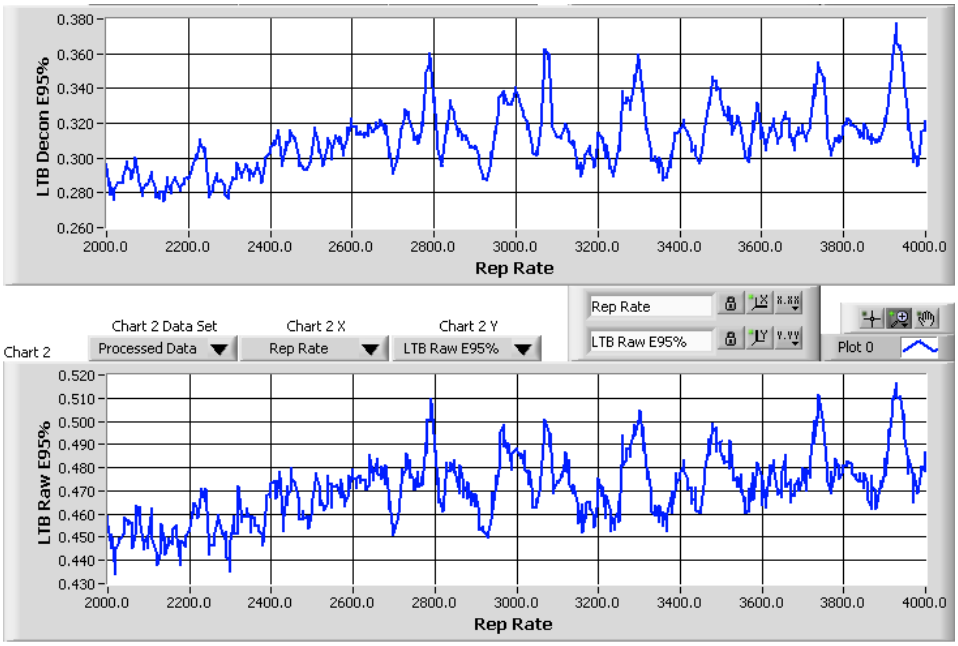

Fig.8. Deconvolved and Convloved E95% measurements of XLA100 output in 2000-4000 Hz range

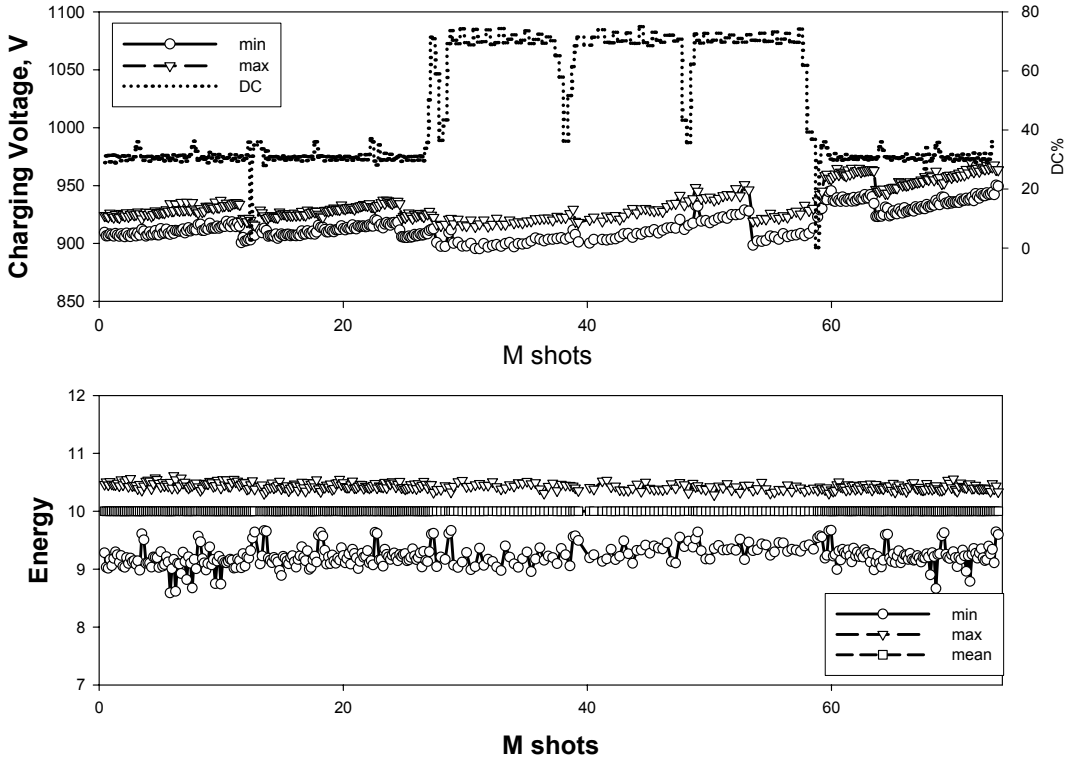

Fig. 9. Variation of output energy and charging voltage over 75M run at 4kHz, various duty cycles

Upper graph shows maximum, mean and minimum operational voltage values measured for samples of 10K shots each
Dotted line shows DC change
Lower graph shows maximum, mean and minimum output energy over 10K shots

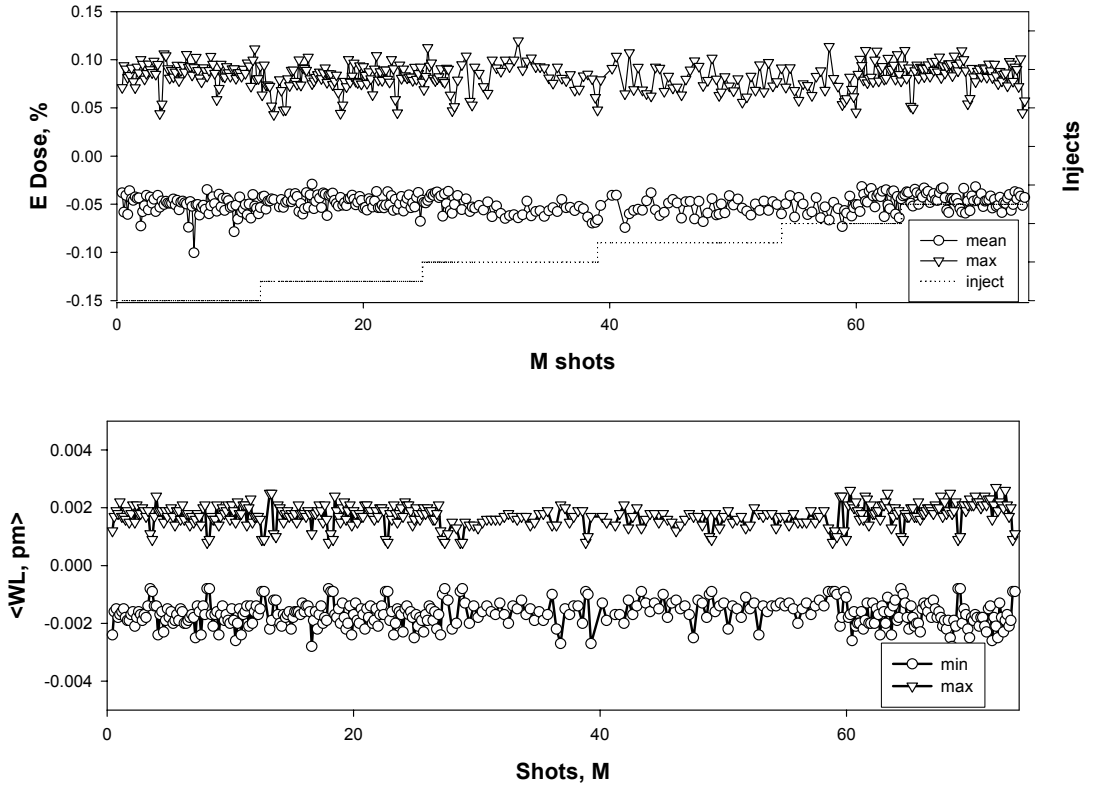

Fig. 10. Energy dose stability and wavelength stability at 4kHz; 80p moving window average applied (burst synchronized), same run as in Fig.9
Upper Graph shows worst energy dose errors for samples of 10K shots each
Dotted line shows F_2 auto injects, made to both chambers.
Lower graph shows wavelength average values for 10K shots

Overall wavelength stability performance of XLA-100 system is similar to the Nanolith 7000A [6]. The PZT-actuator-based wavelength control demonstrates a precise wavelength correction on the pulse-to-pulse basis. The results shown in the bottom graph of Fig.10 illustrate that wavelength average error is maintained within ± 3 fm limits over 75 Mshots run and has a good margin in respect with specified values.

The short-term wavelength stability specification is also applied to the case when the target wavelength is changed *between* the bursts. It this case, the operational wavelength at the first moving average window of the next burst is guaranteed to be within specified error to the new target. For the open loop control operation, the average wavelength error is specified less than 25fm. The maximum wavelength change for the open loop control can be as large as ±0.6pm within a 100ms inter-burst interval. Fig 11 shows the distributions of maximum and minimum window average errors and standard deviation from the average wavelength for 2000 bursts, fired at 4kHz , 100ms inter-burst interval. The target wavelength change was commanded through the laser interface.

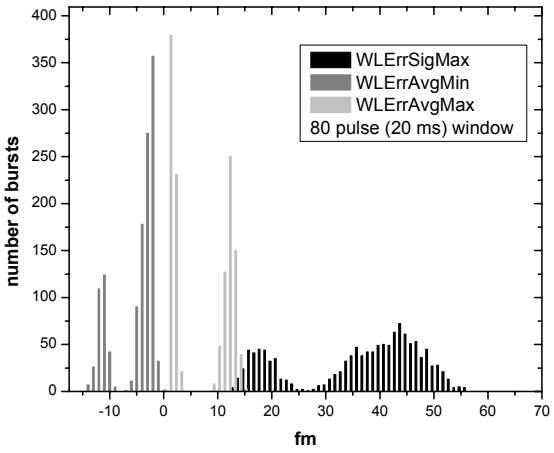

Fig. 11. Histogram of wavelength standard deviation, and minimum and maximum window-average error. Laser operated at 4kHz, burst mode: 200p/0.1s The opened loop wavelength control 0.6 pm target change between each burst 2 steps up, 2 steps down, 2000 bursts were fired

The maximum and minimum window-average in this test are below 20fm. The wavelength standard deviation is less than 56 fm.

TEMPORAL PULSE WIDTH MEASUREMENTS

The 193 nm photon energy is great enough to cause significant damage in projecting lenses and other optical elements in DUV photolithographic exposure tools due to various linear and nonlinear effects. The recent studies on the transmittance properties of fused silica optics under long term irradiation with a 193nm laser source, performed at Cymer [7] indicate that it is important for the 10mJ laser systems to bring the output peak intensity down to equivalent intensity levels of the 5mJ systems, such as Nanolith 7000 (shown in Fig.2). Fig. 12 shows variation of the temporal pulse width over a 100M run at different duty cycles, varied from 6% to 75%. The measurements of the output pulse, were performed with Hamamatsu R132U-54 photodiode and captured by TDS-3054 Tektronix digital oscilloscope (500Mhz, 5Gs/s). The temporal pulse width in Fig 12 was defined as integral-square pulse width:

$$IS = \frac{(\int T(t)dt)^2}{\int T^2(t)dt},$$

where t-time, T(t)-the temporal profile intensity as a function of time[6].

Our studies of the temporal pulse width on MOPA systems show that IS value of the un-stretched pulse, measured directly at PA output is close to IS value of the amplified stimulation emission (ASE) at PA output (MO input is blocked). However the MO temporal pulse shape can also affect the temporal pulse width of MOPA output, which is longer than ASE [2] temporal width. As a result, the pulse width of the XLA-100 output is affected by PA and MO gains due to variation of F_2 concentration and charging voltage changes over a long run. The results in Fig 12 illustrate that IS values meet specifications and maintained flat at ~50ns level over a 100M shots run. The accuracy of the F_2 auto-injects play an important role to maintain long-term stability of IS.

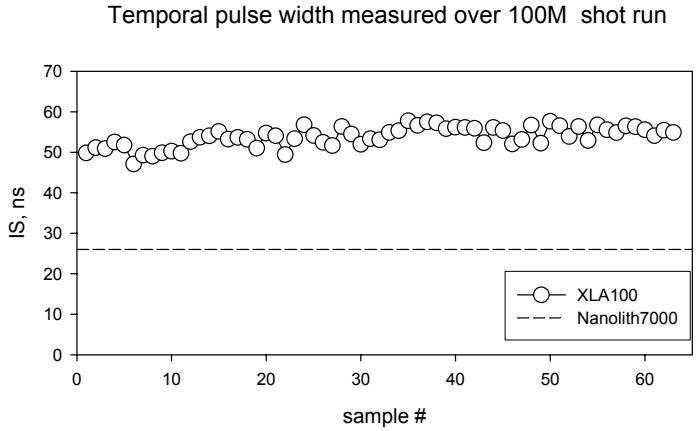

Fig.12. Results of TIS measurements for a 100M run at 4kHz.
the duty cycle is varied between 6% and 75% during the run.
The measurements were taken with ~ 20min intervals

CONCLUSION

Critical optical parameters of XLA100 system, including energy stability, bandwidth, wavelength stability and temporal pulse width are evaluated and meet specifications with long-term runs at various duty cycles. The architectural features of the XLA-100 are discussed. MOPA architecture not only enables ultra line-narrowed, high power, deep ultraviolet radiation, but it also results in a significant reduction of consumable costs. The high pulse energy operation of the XLA-100 system results in a net reduction in pulses fired for each exposure. Additionally, MOPA performance extends consumable module lifetime by improving thermal management, lowering voltage rise levels, reducing chamber electrode wear, optimizing chamber gas mixtures, and increasing operational margins.

Implementation of MOPA dual-chamber technology will provide semiconductor chip manufacturing with unprecedented levels of spectral bandwidth performance, output power generation, and cost savings enabling >0.9NA lithography tool lens designs.

REFERENCES

1. G. Rylov, "F2 MOPA: Some Aspects of Spectral Purity," 3rd International Symposium on 157nm Lithography, 3-6 September 2002, Antwerp, Belgium.

2. Daniel J. W. Brown, Vladimir Fleurov, Alex Ershov, Fedor Trintchouk "New DUV Light Source Breaks Lithography Barriers", 2003, Semicon, Japan

3. V. Fleurov, T. Duffey, G.M. Blumenstock, P. Newman, X.J. Pan, T. Watson, "The New Generation of High Repetition Rate Lasers for sub-100nm Lithography," Paper IB01-04 in Digest of Technical Papers, SEMICON Taiwan 2001.

4. J. Martin Algots, Richard Sandstrom, William Partlo, Petar Maroevic,
Eric Eva, Michael Gerhard, Ralf Lindner, Frank Stietz "Compaction and Rarefaction of Fused Silica with 193-nm Excimer Laser Exposure", Optical Microlithography XVI, 2003, 23-28 February 2003, Santa Clara, CA, USA

5. R. Sandsrom, A. Ershov, V. Fleurov, "MOPA Laser Architecture for High Power Lithographic Light Sources" SPIE 27'th Conference on Microlithography, March 3-8, 2002, Santa Clara, A*C, USA*

6. P.C. Oh, V. Fleurov, T. Hofmann, T. Duffey, F. Trintchouk, P.O'Keeffe, P. Newman, G.M. Blumenstock, " Production ready 4kHz ArF Laser for 193nm Lithography, Optical Microlithography XV, 2002, SPIE, Volume 4691, p.1753-1760

7. R. Sandstrom, *Proc. of 2nd Symposium on 193nm Lithography,* Colorodo Springs, CO, 1997; R. Sandstrom, "Dependence of Compaction in Fused Silica on Laser Pulsewidth at 193 nm", paper E-017,Fourth Intl. Symposium on 193 nm Lithography, Telfs, Austria (Sept., 1998)